

SIMULATION OF THREE PHASE FLOW IN POROUS MEDIA USING A HIGH-RESOLUTION CENTRAL SCHEME

H. Naderan*, M.T. Manzari† and S.K. Hannani††

*Sharif University of Technology, Azadi Ave.
Tehran, Iran

e-mail: h_naderan@mehr.sharif.edu
web page: http://mehr.sharif.edu/~h_naderan

†Sharif University of Technology, Azadi Ave.,
Tehran, Iran

e-mail: mtmanzari@sharif.edu

Key words: Three phase flow, Porous media, High resolution, Central scheme, Unstructured grid

Abstract. *This article aims to demonstrate the advantages of using a high resolution central scheme in the field of multiphase flow in porous media. The black oil model, used in the petroleum reservoir engineering, is employed as it generally provides an acceptable model for most reservoirs and recovery processes.*

The governing equations are split into a parabolic equation for pressure variations and a system of hyperbolic equations for species transport. The hyperbolic part has non-convex degenerate flux functions which presents a major challenge to the robustness of numerical schemes. The two sets of equations are discretized on a triangular unstructured grid. A semi-discrete CFL-independent high-resolution central scheme due to Kurganov and Tadmor is employed in this work.

Two test cases, one with top view and the other with cross sectional view, are solved to assess the performance of the proposed approach. Comparing the obtained results with those of the previous works indicates the robustness and accuracy of the scheme used. The simplicity of derivation and implementation of the numerical method used here makes it a viable choice for dealing with degenerate reservoir problems. Simulations show that inclusion of the gravitational effects in the second test case does not introduce any additional complications in the numerical method. This is in contrast to those schemes which require eigenvalue computations and therefore face substantial difficulty when eigenvalues change dramatically.

1 INTRODUCTION

Numerical simulation of multiphase flow in porous media is an active research area due to its use in analysis of many engineering applications. Oil reservoir simulation is one of

the most important examples of such analyses. The application of advanced numerical schemes in this field has been to some extent, delayed relative to other engineering fields due to the complex nature of the governing equations.

In the petroleum reservoir simulation field, application of one-point upwind scheme for the solution of the saturation equation was popular (Aziz and Settari²). In this method, the flux through the control volume face is calculated from the saturation value of the upstream node and the data from the downstream node is ignored. The excessive diffusion of this method lead to the proposition of a two-point upwind scheme by Todd et al.¹, taking into account two points instead of one in the upstream direction. This scheme is fairly popular especially in commercial simulators. Although these methods have made the solution of the complex behaving governing equations possible, generally their numerical diffusion is high and an excessive grid refinement is needed to obtain a good resolution of the phenomena. Additionally, second-order upwind methods are prone to spurious numerical oscillations near discontinuities. Blunt and Rubin⁷ and Rubin and Edwards¹⁰ proposed Flux Limited schemes to cure this.

Another approach to the problem was the application of high resolution Godunov schemes, initiated by Bell and Shubin³, Bell et al.,⁴, Colella⁸ and Trangenstein and Bell⁶. These methods decompose the equation system according to its eigen-values and eigen-vectors. The contribution of a particular mode from the nodes to the interfacial flux, then depends on the sign of its eigenvalue. If all the eigenvalues happen to have the same sign, the scheme reduces to the upwind schemes mentioned earlier. This is not true in general and as a result, Godunov schemes, compared to upwind schemes, provide a superior resolution in complex flow situations. Due to the degeneracy and non-convexity of the governing equations, the mathematics involved is much more complicated and calculation of eigen-values and eigen-vectors means a greater number of arithmetic calculations per time step. Additionally, when effects such as gravity are included, the eigen-vector structure of the equations are changed and new formulae for calculation of flux contributions needs to be developed (Bell et al.⁵). Extension to two dimensions were achieved by Dicks⁹ on a regular grid and by Bergamaschi et al.¹¹ on a triangular mesh. Although these schemes performed quite well and resolve the flow features with good accuracy, they have not been widely incorporated in the commercial simulators.

Recently a new class of high resolution central schemes due to Kurganov and Tadmor¹² has been applied to the black oil model by Naderan et al.¹⁴. Two major features of this scheme are that it does not require eigen-vector decomposition and independence of its artificial diffusion from the CFL number. The first feature is a major advantage, especially when other strong nonlinear effects like gravity are taken into account and a uniform treatment of such effects is essential. The second feature is helpful in maintaining the accuracy of the scheme on nonuniform grids or when the CFL number is decreased. This is in direct contrast to the general class of central schemes in which excessive amount of diffusion at reduced CFL numbers degrades the quality of solution by for example smearing the sharp fronts.

The present article investigates the application of this scheme and its potential benefits in two dimensional reservoir simulation. The black oil model is used and the governing equations are discretised on a triangular unstructured mesh. The black oil model is a three phase three component model by which, a noticeable number of reservoir and recovery operations can be described. The use of unstructured mesh provides maximum flexibility in local grid refinements, especially near wells. Two different configurations, with and without the effect of gravity are investigated and it is shown that no alteration of the numerical method is needed when the gravity effects are included.

2 Governing equations

Equations governing the black oil model can be formulated in several forms. The form chosen for the present work is based on the work of Trangenstein and Bell⁶, which uses a volume error discrepancy for derivation of the pressure equation. For the sake of brevity, the details of the assumptions and derivation process are not discussed here and only a brief review of the equations is presented.

In the black oil model, the reservoir fluid is considered to be composed of three pseudo-components, which are oil, gas and water, distributed into three phases, liquid, vapor and aqua. Neglecting the capillary effects, all phases have the same pressure, p . The mass of components per pore volume is represented by the vector $\mathbf{z} = \{z_o, z_g, z_w\}^T$ and the volume of each phase by $\mathbf{u} = \{u_l, u_v, u_a\}^T$.

The pressure variation inside the reservoir is governed by the following parabolic equation¹¹:

$$\left(-\phi \mathbf{e}^T \frac{\partial \mathbf{u}}{\partial p} + \mathbf{e}^T \mathbf{u} \frac{\partial \phi}{\partial p} \right) \frac{\partial p}{\partial t} + \mathbf{e}^T \mathbf{u} \frac{\partial \mathbf{u}}{\partial \mathbf{z}} \nabla \cdot (\mathbf{R}\mathbf{B}^{-1}\mathbf{v}) = \frac{\mathbf{e}^T \mathbf{u} - 1}{\Delta t} \phi \quad (1)$$

The vector of phase velocities is defined as

$$\mathbf{v} = \begin{pmatrix} \mathbf{v}_l^T \\ \mathbf{v}_v^T \\ \mathbf{v}_a^T \end{pmatrix}$$

in which

$$\mathbf{v}_j = -\lambda_j (\nabla p - \rho_j \mathbf{g}) \quad (2)$$

are the phase velocities and $\mathbf{v}_t = \mathbf{v}^T \mathbf{e}$ is the total velocity. Moreover, $\mathbf{e} = \{1, 1, 1\}^T$, ϕ is the porosity, ρ_j is density of phase j , \mathbf{g} is the gravitational acceleration vector and t is time. Also, $\lambda_j = K k_{r_j} / \mu_j$ is the mobility of phase j where K is the rock permeability, and k_{r_j} and μ_j are the relative permeability and dynamic viscosity of phase j , respectively.

Summing up both sides of Eq. (2) for all phases, gives the total velocity as follows

$$\mathbf{v}_t = -\lambda (\nabla p - \rho_m \mathbf{g}) \quad (3)$$

where $\lambda = \sum_{j=l,v,a} \lambda_j$ is the total mobility, $\rho_m = \sum_{j=l,v,a} f_j \rho_j$ is the average density and $f_j = \lambda_j / \lambda$. The phase velocities can be written in terms of the total velocity in the following manner;

$$\mathbf{v}_j = f_j \mathbf{v}_t + t_j \mathbf{g} \quad (4)$$

and

$$t_j = f_j \sum_{s \neq j} \lambda_s (\rho_j - \rho_s) \quad (5)$$

The matrix $\mathbf{B} = \text{diag}\{B_l, B_v, B_a\}$, is the volume formation factor which shows the volume of each phase in reservoir condition (RC) compared to the Stock Tank Condition (STC). In the absence of thermal effects, B s are functions of the phase pressure.

The matrix \mathbf{R} is the solution ratio. R_{ij} is defined as the amount of component i in phase j , compared to the amount of principal component of phase j . The principal component of a phase is, by definition, the component present in that phase at STC. Specifically, oil, gas and water are the principal components of the liquid, vapor and aqua phases, respectively.

In the classical black oil model, only the solubility of gas in oil is considered, giving the R matrix the following structure:

$$\mathbf{R} = \begin{bmatrix} 1 & 0 & 0 \\ R_l & 1 & 0 \\ 0 & 0 & 1 \end{bmatrix} \quad R_l = \frac{z_{gl}}{z_{ol}} \quad (6)$$

where z_{ij} is the mass of component i in phase j per pore volume. The model considered by Trangenstein and Bell⁶ is rather more general and considers the solubility of gas in both oil and water and evaporation of oil, with the following \mathbf{R} matrix.

$$\mathbf{R} = \begin{bmatrix} 1 & R_v & 0 \\ R_l & 1 & R_a \\ 0 & 0 & 1 \end{bmatrix} \quad R_l = \frac{z_{gl}}{z_{ol}} \quad R_v = \frac{z_{ov}}{z_{gv}} \quad R_a = \frac{z_{ga}}{z_{wa}} \quad (7)$$

In this work, the general model of Trangenstien and Bell is adopted. The transport of components is governed by the mass conservation law which yields

$$\frac{\partial \phi \mathbf{z}}{\partial t} + \nabla \cdot (\mathbf{R} \mathbf{B}^{-1} \mathbf{v}) = 0 \quad (8)$$

Here, \mathbf{u} and \mathbf{z} are related together by

$$\mathbf{u} = \mathbf{B} \mathbf{T} \mathbf{z} \quad (9)$$

where \mathbf{T} is a matrix such that $\mathbf{T} \mathbf{R} = \mathbf{I}$.

When all the three phases are present, the flow is termed saturated. However, there is a possibility that the gas is completely dissolved into the liquid phase, thus, eliminating

the vapor phase. This situation is called under-saturation which shows that the reservoir pressure is higher than the liquid bubble pressure and the liquid phase has the capacity to swallow more gas. In this case, \mathbf{R} , \mathbf{T} and \mathbf{B} matrices need to be modified but the general form of Eqs. (1), (8) and (9) does not alter. This is the main reason for choosing this formulation as the base of present work, since it permits a unified treatment of the saturated and under-saturated cases. For a detailed discussion of the under-saturated cases, consult Trangenstein and Bell⁶.

3 Numerical method

Discretisation of the governing equations was carried on a triangular unstructured grid. This brings a great amount of flexibility in geometry definition and mesh adaptation.

Figure 1 shows a typical grid node, its neighboring triangular elements and the corresponding control volume. The mesh has a unit depth in the direction normal to the plane. The control volume is constructed around the node using the medians of the elements, shown by thick lines. All the governing equations are discretised on this control volume. For future reference, the line connecting two neighboring nodes is termed as an edge and each segment of thick line on the perimeter of the control volume is called a face.

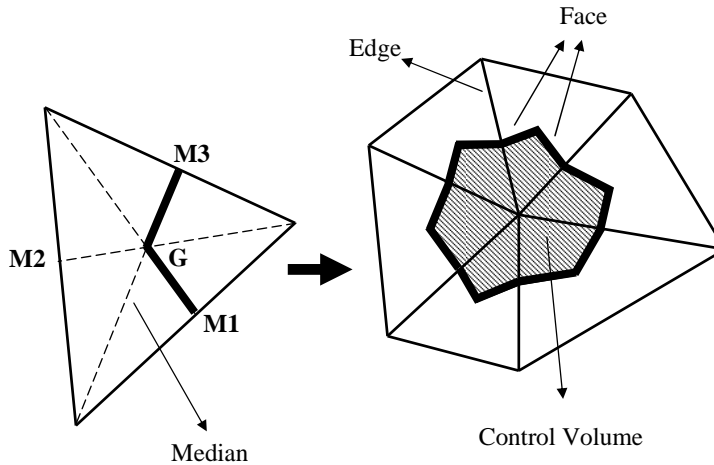


Figure 1: Construction of nodal control volumes in a triangular mesh

As a result, the numerical method used, can be identified as a vertex centered FVM. Two faces are associated to each edge, which the numerical fluxes run through. These faces can be unified by vector summing the area vectors normal to the surfaces (Fig. 2).

Using this, the number of flux calculations will be equal to the number of edges, which is half the number of the original control surfaces. Integrating Eq. (1) on the control volume shown in Fig. 1, using an implicit approach in time gives

$$\iiint \alpha \frac{\partial p}{\partial t} d\mathcal{V} dt + \iiint \mathbf{e}^T \mathbf{B} \mathbf{T} \nabla \cdot (\mathbf{R} \mathbf{B}^{-1} \mathbf{v}) d\mathcal{V} dt = \iiint \beta d\mathcal{V} dt \quad (10)$$

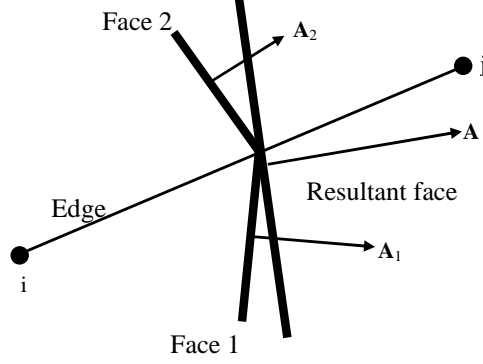


Figure 2: Unification of control surfaces

where

$$\alpha = -\phi \mathbf{e}^T \frac{\partial \mathbf{u}}{\partial p} + \mathbf{e}^T \mathbf{u} \frac{\partial \phi}{\partial p}$$

$$\beta = \frac{\mathbf{e}^T \mathbf{u} - 1}{\Delta t} \phi$$

Assuming that p is constant over the control volume, \mathbf{RB}^{-1} in the second term is treated as a constant, simplifying Eq. (10) to the following form

$$\alpha_i (p_i^{n+1} - p_i^n) \mathcal{V} + \Delta t \sum_{j \in N(i)} \mathbf{v}_{ij}^{n+1} \cdot \mathbf{A}_{ij} = \beta_i \mathcal{V} \Delta t \quad (11)$$

The coefficients α and β are evaluated at time t_n while the total velocities are evaluated at time t_{n+1} . $N(i)$ is the set of neighboring nodes for node i , \mathcal{V} is the volume of control volume i and $(\)_{ij}$ is the property associated to the edge connecting nodes i and j . The velocities belong to the faces and are calculated by discretising Eq. (3) along the edge;

$$\mathbf{v}_{ij} \cdot \mathbf{A}_{ij} = -\lambda_{ij} \frac{p_j - p_i}{|\mathbf{r}_{ij}|} \hat{\mathbf{r}}_{ij} \cdot \mathbf{A}_{ij} + \frac{1}{2} \lambda_{ij} (\rho_{mi} + \rho_{mj}) \mathbf{g} \cdot \mathbf{A}_{ij} \quad (12)$$

in which \mathbf{r}_{ij} is the vector connecting i to j and $\hat{\mathbf{r}}_{ij}$ is the unit vector along the edge. λ_{ij} is the equivalent mobility of the edge and is calculated by harmonic averaging the values from nodes i and j .

For the component transport, integration over the control volume using an explicit time approximation yields

$$\mathbf{z}_i^{n+1} - \mathbf{z}_i^n = -\frac{\Delta t}{\phi_i \mathcal{V}} \sum_{j \in N(i)} \mathbf{h}_{ij}^n \cdot \mathbf{A}_{ij} \quad (13)$$

where \mathbf{h}_{ij}^n is the flux vector $\mathbf{RB}^{-1} \mathbf{v}$ of edge ij , evaluated on its corresponding face, and can be written as a function of the conserved variables on the two sides of the face. This

is an essential element of this work as the type of this function has a direct impact on the resolution and accuracy of the results. The approach taken here is adopted from the work of Kurganov and Tadmor¹², Kurganov and Petrova¹³ and Naderan et al.¹⁴. The original work of Kurganov and Tadmor was formulated in both semi and fully-discrete forms. Here, the semi-discrete form is used since it is already in the conservation form. The same expression for the face flux can be reached from the fully-discrete form with some algebraic manipulations. This method has an artificial diffusion of order $O(\delta^3)$ where δ is an element size indicator¹². The numerical flux is given by

$$\mathbf{h}_{ij} \cdot \mathbf{A}_{ij} = \frac{1}{2} [\mathbf{h}_n^+ + \mathbf{h}_n^-] - \frac{1}{2} a_{ij} A_{ij} (\mathbf{z}^+ - \mathbf{z}^-) \quad (14)$$

in which

$$\begin{aligned} \mathbf{z}^+ &= \mathbf{z}_j - \frac{1}{2} \psi_j(\mathbf{z}_i) \nabla \mathbf{z}_j \cdot \mathbf{r}_{ij} \\ \mathbf{z}^- &= \mathbf{z}_i + \frac{1}{2} \psi_i(\mathbf{z}_j) \nabla \mathbf{z}_i \cdot \mathbf{r}_{ij} \end{aligned}$$

are the right and left states, respectively, and \mathbf{h}_n^\pm is $\mathbf{R}\mathbf{B}^{-1}\mathbf{v} \cdot \mathbf{A}_{ij}$, evaluated by substituting the pressure of the edge midpoint and \mathbf{z}^\pm . Figure 3 shows the quantities defined above. $\psi(\mathbf{z}_i)$ is the slope limiter defined by

$$\psi_i(\mathbf{z}_j) = \min \left[1, \gamma \frac{\min(\mathbf{M}_i - \mathbf{z}_j, \mathbf{z}_j - \mathbf{m}_i)}{\max|\nabla \mathbf{z}_i \cdot \mathbf{r}_{ik}|} \right] \quad (15)$$

in which $k \in N(i)$. $\mathbf{m}_i = \{m_{oi}, m_{gi}, m_{wi}\}^T$ and $\mathbf{M}_i = \{M_{oi}, M_{gi}, M_{wi}\}^T$ are defined as follows:

$$\begin{aligned} m_{li} &= \min(z_{li}, z_{lk}) \\ M_{li} &= \max(z_{li}, z_{lk}) \\ l &= o, g, w \end{aligned}$$

For $\gamma = 1/2$ the limiter is the two dimensional extension of the well-known minmod limiter, which is used in this work.

a_{ij} is defined as

$$\rho \left(\frac{\partial \mathbf{h}}{\partial \mathbf{z}}(\mathbf{z}) \right) \quad \mathbf{z} \in \mathcal{C}(\mathbf{z}^-, \mathbf{z}^+) \quad (16)$$

where $\rho(\mathbf{X})$ is the spectral radius of matrix \mathbf{X} and $\mathcal{C}(\mathbf{z}^-, \mathbf{z}^+)$ is a path that connects the two states $\mathbf{z}_{1+1/2}^-$ and $\mathbf{z}_{1+1/2}^+$ in the phase space via Riemann fans.

Since the flux function is non-convex and complicated to evaluate, it is not easy or even sometimes possible to find a_{ij} accurately. In the present work, the following estimate is used

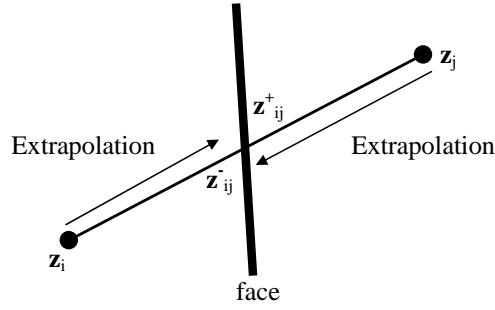


Figure 3: Extrapolation of nodal values to face

$$a_{ij} = \rho \left(\frac{\partial \mathbf{h}}{\partial \mathbf{z}}(\bar{\mathbf{z}}) \right) \quad (17)$$

in which $\bar{\mathbf{z}}$ is the arithmetic mean of \mathbf{z}^- and \mathbf{z}^+ . Numerical experiments proved that this is sufficiently close to the true maximum wave speed.

The CFL condition is computed on the basis of wave speed, a , and a global CFL number, C , at each face, using

$$\frac{a_{ij} \Delta t}{\Delta x} < C \quad (18)$$

In practice, a global time-step size is used which is the minimum of allowable time-steps computed for each cell in the grid.

4 Test cases

To assess the performance of the method mentioned above, two test cases are solved, each showing a different aspect of the method. Both test problems are chosen from Dicks⁹.

The first test case, is the typical five spot configuration, shown in Fig. 4. The side of the square is $100ft$. The domain is divided into 3200 triangular elements, giving roughly 1600 nodes which is the same number of nodes used by Dicks. A regular triangulation was avoided in order to rule out any effect of grid orientation on the solution. Initially, the reservoir has a composition of $\mathbf{z}_{resv} = \{0.703, 70.3, 0.0502\}^T$ and a pressure of $1800psi$. Injection takes place at the lower left corner with a mixture composition of $\mathbf{z}_{inj} = \{0.0414, 66.23, 0.497\}^T$ at $2000psi$. Production is carried out at the upper right corner with a pressure of $1600psi$. All the model parameters are defined in the appendix A.

This problem has an areal view hence, gravity plays no roll in the flow. The initial state of the reservoir is saturated and a saturated mixture is injected into it. This test problem shows the general structure of the flow when all the three phases are present.

The second test case is a cross sectional problem in the $x-z$ plane. The domain consist of a $400 \times 50ft^2$ rectangle divided into 1330 triangular elements (Fig. 5). Gravitational

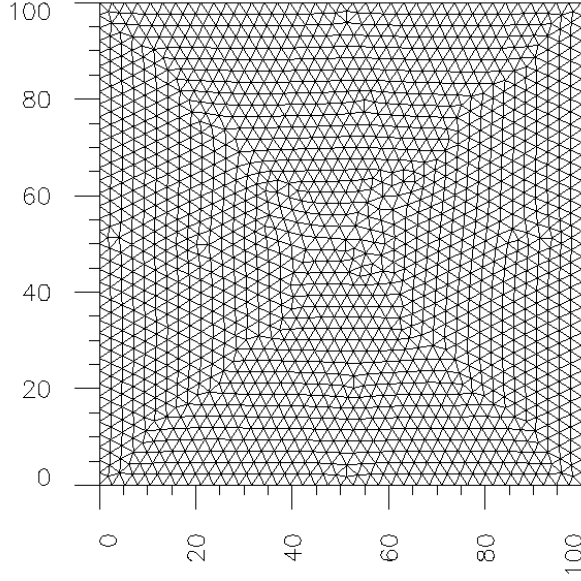


Figure 4: Computational grid used for test case 1

acceleration is acting vertically downwards with a magnitude of $32.2 ft/s^2$. The initial reservoir pressure is $1800 psi$ and has a hydrostatic distribution throughout the domain. Injection takes place from the entire left boundary and has a pressure of $2000 psi$ at the top with a hydrostatic distribution along the edge. Production is along the right side with a constant pressure of $1600 psi$ over the entire edge. Since the pressure is variable in the domain, a constant value for composition cannot be defined. Instead the value of saturation in the reservoir and at the injection boundary is specified and composition is calculated from the hydrostatic distribution condition. The initial reservoir saturation is $\mathbf{s}_{resv} = \{1.0, 0.0, 0.0\}^T$ with a bubble pressure of $1800 psi$. The injected fluid saturation is $\mathbf{s}_{inj} = \{0.0, 0.0, 1.0\}^T$. The model parameters are the same as test case 1.

It is notable that although free gas is not present, the value of bubble pressure reveals that the gas component is present and is totally dissolved in the liquid phase. Hence the reservoir initial state is undersaturated. As the flow develops, reduction of pressure in regions near the production boundary will make the gas leave the liquid phase and appear as free gas making the flow a mixed saturated/undersaturated type. Furthermore, due to the small density of the free gas, relative to the other two phases, and the presence of gravitational forces, the vapor phase tends to raise quickly and percolate at the top of the domain. Although the test case configuration is simple, the complex nature of this flow places a tough test on the stability and accuracy of the method when nonlinearities are severely increased.

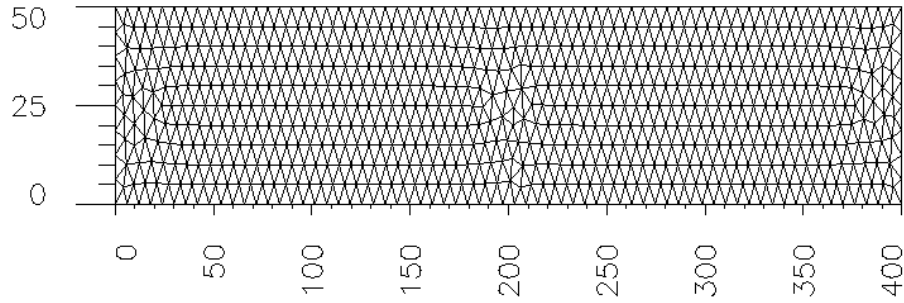


Figure 5: Computational grid used for test case 2.

5 Results and discussion

Figures 6-9 show a side by side comparison of the results obtained in the current work (left side) and the work of Dicks⁹ (right side). Both sets of figures show the reservoir after 5 days of injection. As can be seen, the structure of the waves and their fronts are in good agreement. The slight discrepancy between the front shapes can be associated to the regular shape of the grids used by Dicks and the irregular shape of the control volumes used in this work.

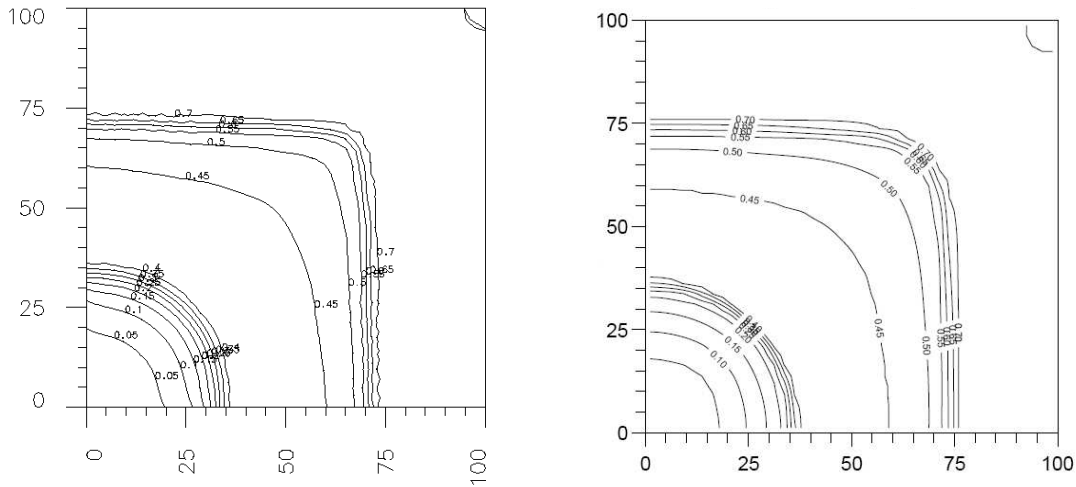


Figure 6: Oil component density in test case 1. left: current work, right: work of Dicks⁹

Figure 10 shows the structure of the waves at day 5. The z axis represents the saturation percentage of each phase. At any point on the $x - y$ plane, the distance from the ground to the first surface indicates the saturation of the vapor phase, the distance from the first surface to the second surface indicates the saturation of the liquid phase and the rest of the height shows the saturation of the aqua phase. The sum of the three saturations is 100% which is the total height of the graph.

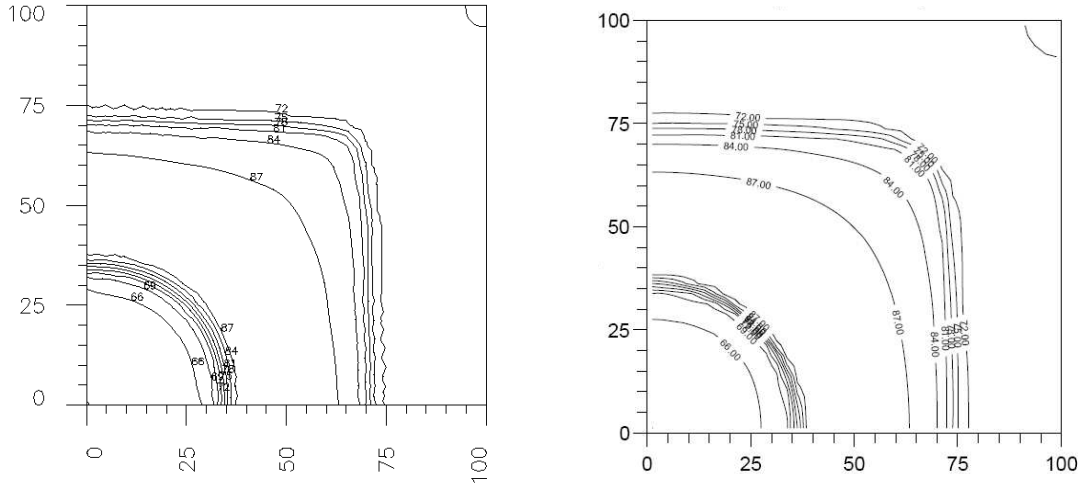


Figure 7: Gas component density in test case 1. left: current work, right: work of Dicks⁹

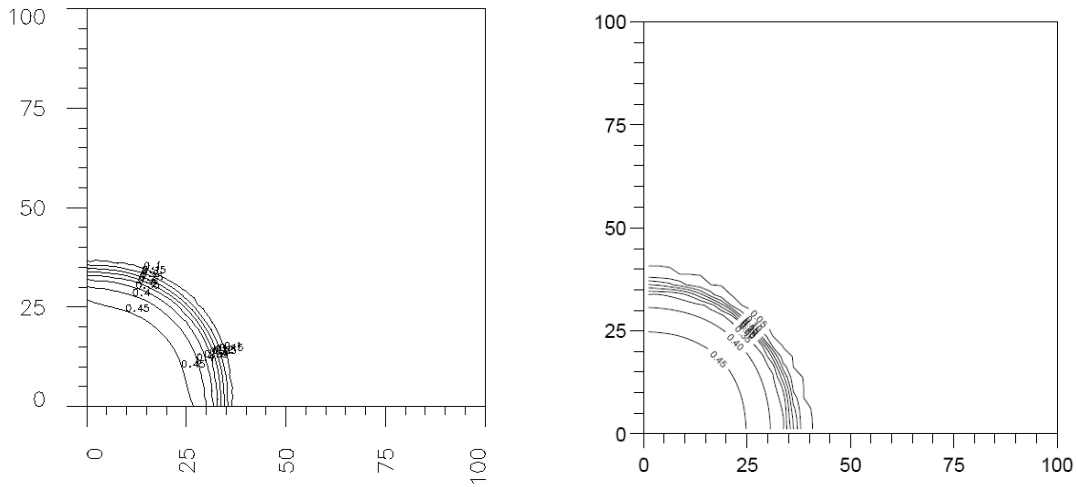


Figure 8: Water component density in test case 1. left: current work, right: work of Dicks⁹

As it is clear, injection initiates two fronts, one of them moves faster than the other. The faster front is associated to the gas movement as it is more mobile. The complexity of the solution can be envisaged from the shock-rarefaction form of the faster running wave.

Figures 11-14 give the results of current work (upper tiles) and the results from Dicks⁹ (lower tile) for test case 2. Both sets of figures, give a snapshot of the reservoir at day 15 from the start of injection. The figures show clearly that both methods predict the reservoir state quite similarly. The water-oil front in Fig. 11(top) is slightly sharper than that of Fig. 11(bottom) which can be associated to the higher number of elements used.

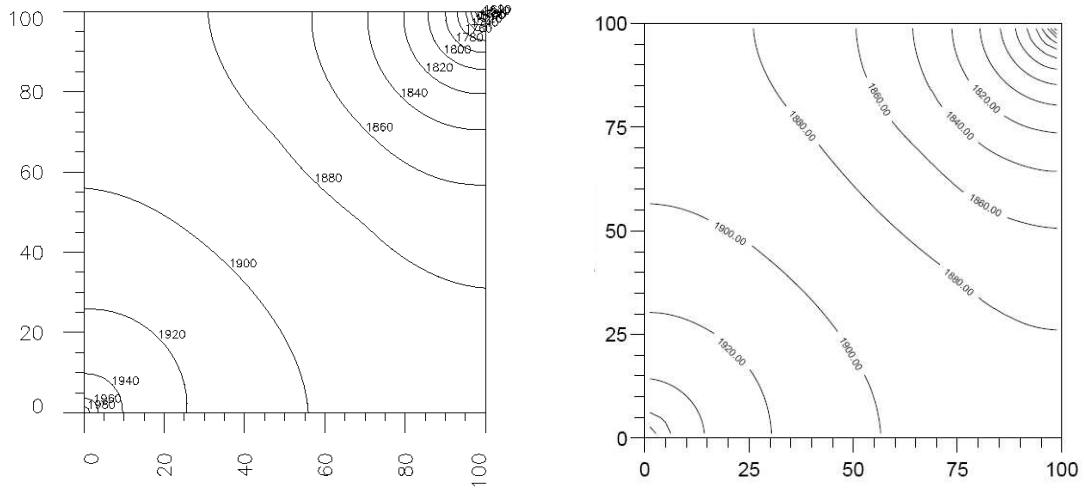


Figure 9: Pressure distribution in test case 1. left: current work, right: work of Dicks⁹

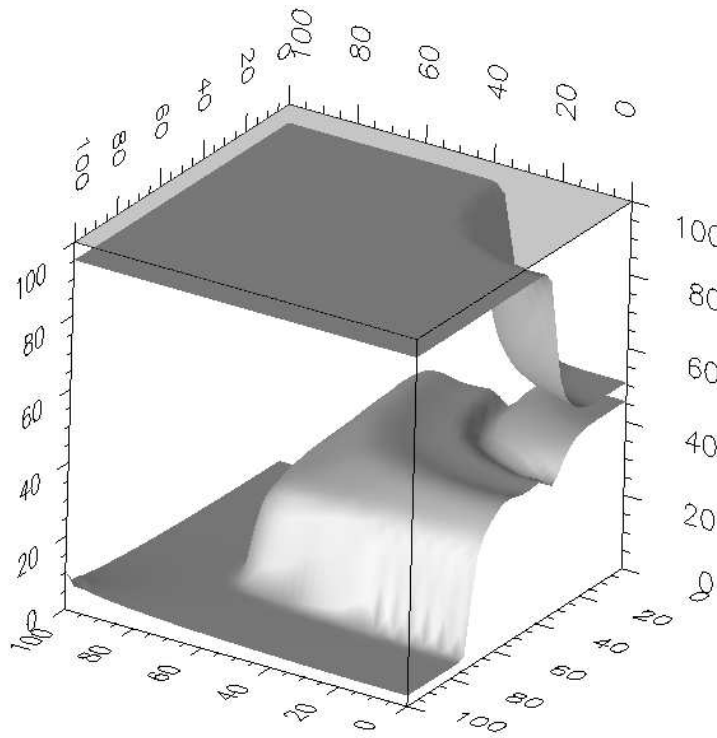


Figure 10: A three dimensional graph of the wave structure of the flow in test case 1. The distance between the ground and the lower surface is the vapor phase, between the lower and upper surface is the liquid phase and between the upper surface and top is the aqua phase saturation

Furthermore, Dicks⁹ has compared his results in this test case with the results obtained

from VIP, a well established commercial reservoir simulator. This gives a double check on the current method.

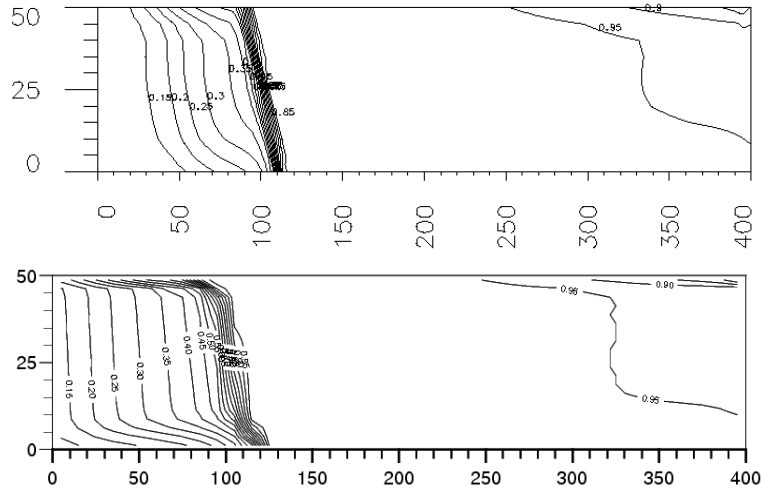


Figure 11: Saturation of the liquid phase in test case 2. top: current work, bottom: work of Dicks⁹

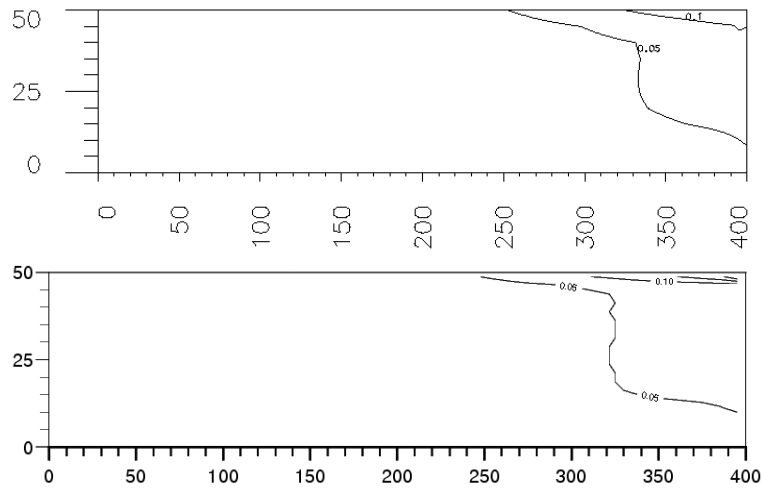


Figure 12: Saturation of the vapor phase in test case 2. top: current work, bottom: work of Dicks⁹

Figure 12 shows the liberation of gas and its percolation in top of the domain. It can be seen that the higher order Godunov method which uses a rigorous eigenvector decomposition and the current method which uses a much simpler analysis virtually give the same result.

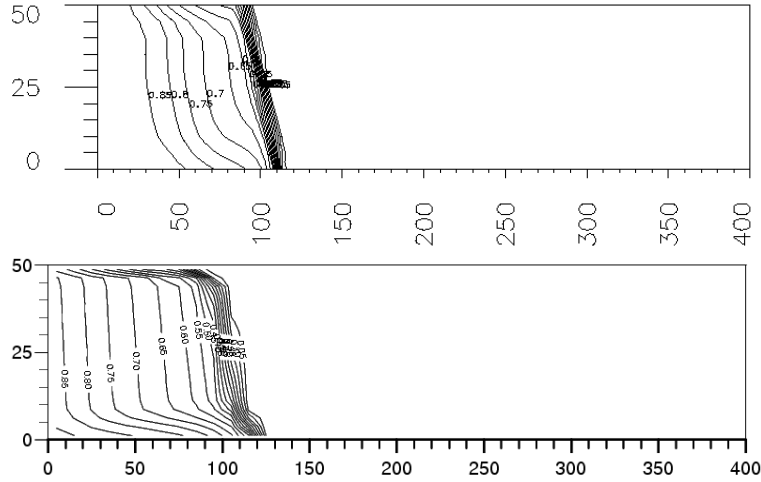


Figure 13: Saturation of the aqua phase in test case 2. top: current work, bottom: work of Dicks⁹

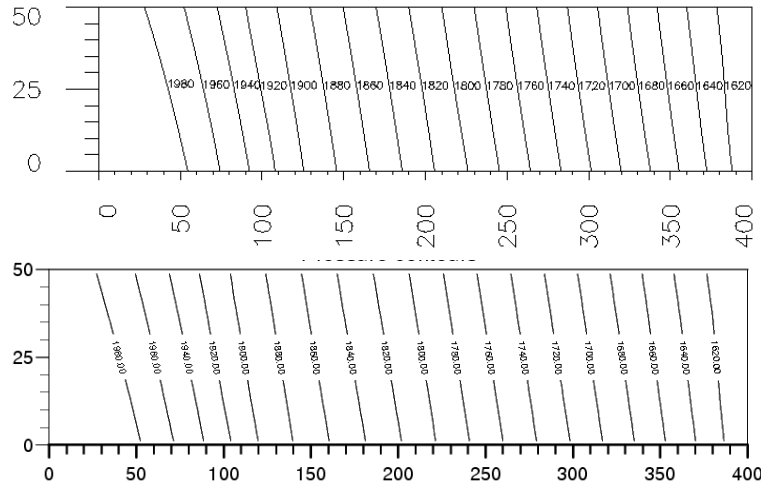


Figure 14: Pressure distribution in test case 2. top: current work, bottom: work of Dicks⁹

6 Conclusion

In the present work, a new form of high resolution central schemes, originally developed for compressible flow computations, was successfully applied to the problem of three phase flow in porous media. The extension is made to two dimensional problems using unstructured grids. The results show that the method meets the expectations set by other more sophisticated methods in terms of accuracy.

The scheme can handle mixed saturated/undersaturated flow seamlessly, with no change in formulation or solution variables. Moreover, it was shown that effects such as gravity can be taken into account with minimal effort.

The simplicity in mathematical formulation and implementation of the numerical method, besides robustness in complex flow situations, make this method a good candidate for solving practical problems.

REFERENCES

- [1] M.R. Todd, P.M.O'Dell and G.J. Hirasaki. Methods for increased accuracy in numerical reservoir simulators. *Trans. SPE of AIME*, **253**, 515–530, (1972).
- [2] K. Aziz and A. Settari. *Petroleum reservoir simulation*, Elsevier Applied Science Publishers, (1979). .
- [3] J.B. Bell and G.R. Shubin. Higher order Godunov method for reducing numerical dispersion in reservoir simulation. *SPE 13514*, 179–186, (1985).
- [4] J.B. Bell, G.R. Shubin and J.A. Trangenstein. A method for reducing numerical dispersion in two-phase black-oil reservoir simulation. *J. Comput. Phys.*, **65**, 71–106, (1986).
- [5] J.B. Bell, P. Colella and J.A. Trangenstein. Higher order Godunov methods for general system of hyperbolic conservation laws. *J. Comput. Phys.*, **82**, 362–397, (1989).
- [6] J.A. Trangenstein and J.B. Bell. Mathematical structure of thye black-oil model for petroleum reservoir simulation. *SIAM J. Appl. Math.*, **49(3)**, 749–783, (1989).
- [7] M.Blunt and B.Rubin. Implicit flux limiting schemes for petroleum reservoir simulation. *Proc. 2nd European Conf. on the Math. of Oil Recov.*, Editions Technip, Paris, 131–138, (1990).
- [8] P. Colella. Multidimesional upwind methods for hyperbolic conservation laws. *J. Comput. Phys.*, **87**, 171–200, (1990).
- [9] M.E. Dicks. *Higher order godunov Black-oil simulations for compressible flow in porous media*, Ph.D. thesis, University of Reading, Reading, UK, (1993).
- [10] B. Rubin and M. Edwards. Extension of the TVD midpoint scheme to higher order accuracy. *Proc. 12th SPE Sympos. Reserv. Sim.*, New Orleans, SPE paper 25265, (1993).
- [11] L. Bergamaschi, S. Mantica and G. Manzini. A mixed finite element-finite volume formulation of the black-oil model. *SIAM J. Sci. Comput.*, **20(3)**, 970–997, (1998).
- [12] A. Kurganov and E. Tadmor. New high-resolution central schemes for nonlinear conservation laws and convection-diffusion equations. *J. Comput. Phys.*, **160**, 241–282, (2000).

- [13] A. Kurganov and G. Petrova. Central-upwind schemes on triangular grids for hyperbolic systems of conservation laws. *Numerical Methods for Partial Differential Equations*, **21**, 536–555, (2005).
- [14] H. Naderan, M.T. Manzari and S.K. Hannani. Application and performance comparison of high resolution central schemes for the black-oil model. *submitted for publication*, (2005).

A Properties of rock and fluids

The spatial coordinates have units of feet, and time t is measured in days. Pressure p is measured in psi, viscosity is measured in centipoise and the rock permeability K is measured in 0.006328 times the value in millidarcies. In this work, $K = 100md$ and porosity $\phi = 0.2(1 + 10^{-5}p)$.

The relative permeability functions are

$$\begin{aligned} k_{r_l} &= (1 - s_v - s_a)(1 - s_v)(1 - s_a) \\ k_{r_v} &= s_v^2 \\ k_{r_a} &= s_a^2 \end{aligned}$$

The solution ratios are given as

$$\begin{aligned} R_l(p) &= 0.05p \\ R_v(p) &= 9 \times 10^{-5} - 6 \times 10^{-8}p + 1.6^{-11}p^2 \\ R_a(p) &= 0.005p \end{aligned}$$

Viscosities are defined by

$$\begin{aligned} \mu_l &= \begin{cases} 0.8 - 10^{-4}p & \text{saturated liquid} \\ (0.8 - 10^{-4}p_b)(1 + 6.78 \times 10^{-5}(p - p_b)) & \text{undersaturated liquid} \end{cases} \\ \mu_v &= 0.012 + 3 \times 10^{-5}p \\ \mu_a &= \begin{cases} 0.35 & \text{saturated aqua} \\ 0.35(1 + 6.78 \times 10^{-5}(p - p_b)) & \text{undersaturated aqua} \end{cases} \end{aligned}$$

and finally, the volume formation factors are

$$\begin{aligned} B_l &= \begin{cases} 1.0 - 2.31 \times 10^{-5}p & \text{if } R_l(p) \equiv 0 \\ 1.0 + 1.5 \times 10^{-4}p & \text{saturated liquid} \\ \frac{1.0 + 1.5 \times 10^{-4}p_b}{1.0 + 2.31 \times 10^{-5}(p - p_b)} & \text{undersaturated liquid} \end{cases} \\ B_v &= \begin{cases} \frac{1}{6.0 + 0.06p} & \text{saturated vapor} \\ \frac{1}{7.0 + 0.06p} + \frac{\bar{R}_v}{R_v} \left[\frac{1}{6.0 + 0.06p} - \frac{1}{7.0 + 0.06p} \right] & \text{undersaturated vapor} \end{cases} \\ B_a &= \begin{cases} 1.0 - 1.8 \times 10^{-5}p & \text{if } R_a(p) \equiv 0 \\ 1.0 - 3 \times 10^{-6}p & \text{saturated aqua} \\ \frac{1.0 - 3 \times 10^{-6}p_b}{1.0 + 6.87 \times 10^{-5}(p - p_b)} & \text{undersaturated aqua} \end{cases} \end{aligned}$$